

Infrared Emission from Intracluster Dust Grains and Constraints on Dust Properties

Kenkichi YAMADA and Tetsu KITAYAMA

Department of Physics, Toho University, Funabashi, Chiba 274-8510, Japan

yamada@ph.sci.toho-u.ac.jp

(Received 2005 March 31; accepted 2005 June 6)

Abstract

For 117 clusters of galaxies, we explore the detectability of intracluster dust grains by current and future infrared facilities, taking into account both collisional heating and sputtering of grains by ambient plasma. If the dust grains are injected into the intergalactic space with the amount and size comparable to the Galactic values, the dust-to-gas ratio is typically 10^{-6} and the mean dust temperature is ~ 30 K near the cluster center. The predicted infrared intensities lie marginally above the detection thresholds for Spitzer Space Telescope, ASTRO-F, Herschel and SPICA missions. For some nearby clusters such as Perseus, A3571, A2319, A3112 and A2204, good detections of intracluster dust signal are expected in the $70\ \mu\text{m}$ band. Given rather tight constraints on the dust temperature from observed electron density and temperature, the dust mass can be inferred directly from the infrared observations. Further constraints on the size distribution will be obtained once multi-band data are available. They will definitely provide a powerful probe of the dust injection processes and dust-gas interactions in the intergalactic space.

Key words: ISM: dust, extinction — galaxies: clusters: general — galaxies: intergalactic medium — infrared: general — X-rays: galaxies: clusters

1. Introduction

Dust grains have so far been detected only in the interstellar medium and there is no firm detection in the intergalactic medium. The presence of dust grains in the latter region is still an open question. If they exist, the intergalactic dust grains should have great impacts not only on our understanding of galaxy evolution but also on our interpretation of high redshift observational data. From X-ray measurements of heavy metal lines, it is evident that there is a significant amount of metal outside of galaxies in clusters and groups of galaxies (e.g., Mushotzky et al. 1996; Renzini 1997; Davis, Mulchaey & Mushotzky 1999; Buote 2000). Such elements are likely to have been expelled out of galaxies through supernova explosion, ram pressure stripping, or tidal interaction. Dust could also be expelled by these processes or by some independent mechanism such as radiation pressure (e.g., Chiao & Wickramasinghe 1972; Ferrara et al. 1991; Shustov & Vibe 1995; Davies et al. 1998; Simonsen & Hannestad 1999; Aguirre et al. 2001a,b)

When dust grains are placed in the intracluster medium (hereafter ICM), they would be heated by collisions with ambient hot X-ray emitting electrons and ions, and emit mainly in infrared bands (Dwek et al. 1990). At the same time, they are destructed via collisions with impinging ions (sputtering) with a typical timescale of $\sim 10^8$ yr. The intracluster dust (hereafter ICD), if any, will therefore provide a direct clue to the ejection processes of materials from galaxies. Indeed, diffuse dust before destruction has been detected in a number of elliptical galaxies (e.g. Goodfrooij & de Jong 1995). The temperature,

the amount, and the size distribution of the ICD, however, can be quite different from those in the interstellar medium; in the absence of stellar photons, temperature of the ICD will be lower than that in elliptical galaxies. Moreover the ICD may be an important cooling agent in the ICM (Montier & Giard 2004). Revealing the nature of the ICD will be of particular importance in understanding the dust-gas interaction.

There have been several suggestions and debates regarding the presence of the intergalactic dust. For example, Girardi et al. (1992) suggested that the redshift asymmetries of member galaxies in nearby groups are consistent with the presence of dust in the intragroup medium. The observed oxygen K edge in an X-ray spectrum of the Perseus cluster may also be attributed to the ICD (Arnaud & Mushotzky 1998). The extended submillimeter emission detected in a rich galaxy cluster may partly be due to dust (Komatsu et al. 1999; Kitayama et al. 2004). On the other hand, the presence of enhanced visual extinction towards high redshift objects behind clusters is still controversial (e.g., Maoz 1995).

More direct evidence has been searched for in the far-infrared bands. Hickson et al. (1989) report that the far-infrared emission is enhanced by a factor of 2 in compact groups of galaxies compared with a sample of isolated galaxies. Sulentic & De Mello Rabaca (1993), however, point out that the results of Hickson et al. (1989) are likely to have been overestimated mainly due to the limited spatial resolution of IRAS. The emission statistically detected in the IRAS data with many clusters of galaxies may partly be due to the ICD (Montier & Giard 2005). Stickel et al. (1998 and 2002) observed 6 galaxy

clusters with ISOPHOT, and only in Coma they reported the excess of ~ 0.2 MJy/sr at $120\ \mu\text{m}$ towards the central region. They estimated the dust color temperature of $T_{\text{d}} \sim 30$ K, the excess flux of $F_{\text{ICD}} \sim 2.8$ Jy and dust mass of $M_{\text{d}} \sim 10^7 M_{\odot}$ from the ratio of surface brightness at $120\ \mu\text{m}$ and $180\ \mu\text{m}$. The visual extinction derived from the dust mass is a negligible amount ($A_{\text{V}} \ll 0.1$ mag). The result is in contrast to the reported optical extinction of ~ 0.3 mag for Coma (Zwicky 1962, Karachentsev & Lipovetskii 1969).

The major difficulties in the past infrared observations are the limited sensitivity and spatial resolution of the detector. The observational data thus might be affected by Galactic cirrus emission, contamination of individual galaxies, and confusion of extragalactic sources. The infrared instruments on the current and future missions, such as Spitzer Space Telescope, ASTRO-F, Herschel, and SPICA, possess much improved sensitivity and spatial resolution that are essential for separating the ICD emission from the other components.

In this paper, we explore the possibility of detecting the ICD with Spitzer Space Telescope, ASTRO-F, Herschel and SPICA by performing a comprehensive study of the expected intensities from the ICD for 117 clusters of galaxies at redshift $z \sim 0.01 - 0.8$. Based on currently available X-ray data, we explicitly take into account both heating and sputtering of dust grains via collisions with ambient hot plasma to compute their temperature and size distributions. We further examine the expected constraints from the near future observations on underlying dust model.

This paper is organized as follows. We describe our sample of galaxy clusters in Section 2. Details of the model for the ICD size distribution is presented in Section 3. Section 4 describes the results for the properties of the ICD and the expected infrared spectra, as well as constraints from future observations on underlying dust model. We discuss several uncertainties in the present analysis in Section 5. Finally, Section 6 summarizes our conclusions. Throughout the paper, we assume a standard set of cosmological parameters; $\Omega_{\text{m}} = 0.3$, $\Omega_{\Lambda} = 0.7$, $\Omega_{\text{b}} = 0.04$, and $h = 0.7$.

2. Sample clusters

In order to calculate the ICD emission, we pick up 117 clusters at redshift $z \sim 0.01 - 0.8$ for which gas properties can be determined by X-ray spectroscopy and imaging data from ROSAT and ASCA. Unless stated otherwise, we adopt an isothermal β -model for the gas density profile of clusters.

We extract 79 clusters at $z \sim 0.1 - 0.8$ from Ota & Mitsuda (2004). We also supplement the sample with 38 nearby clusters at $z \sim 0.01 - 0.1$ from Mohr et al. (1999) and White (2000) for which the β -model parameters, temperature, and metalicity are all available. For some clusters, Mohr et al. (1999) fit the X-ray surface brightness by a sum of two β -model profiles. In such cases, we use the Abel's integral to deproject the fitted surface bright-

ness profile into the electron density profile (Yoshikawa & Suto 1999). For the three clusters (A1689, A2204 and PKS0745-19) compiled in both Ota & Mitsuda (2004) and Mohr et al. (1999), we use the parameters from the former paper for definiteness.

3. Model

3.1. Dust-gas interaction

We first need to specify the basic dust model to calculate the ICD emission. We consider a mixture of equal amounts of spherical silicate and graphite as dust components, and adopt as their mass densities $\rho_{\text{gra}} = 2.26\ \text{g cm}^{-3}$ (Draine & Lee 1984) and $\rho_{\text{sil}} = 3.5\ \text{g cm}^{-3}$ (Li & Draine 2001), respectively. Using these two components, the extinction curve in our Galaxy can be well reproduced (Mathis, Rumpl & Nordsieck 1977, hereafter MRN; Draine & Lee 1984; Laor & Draine 1993).

If dust grains exist in the ICM, they will be heated by collision with ambient X-ray emitting hot electrons and ions, and consequently emit in infrared band as they cool. The temperature of the ICD is then obtained via the balance between collisional heating and radiative cooling.

For given gas temperature and density, we determine the temperatures of dust grains following Dwek (1986) taking account of both heating and cooling between each collision. The heat capacities for graphite and silicate are taken from Dwek (1986) and Draine & Anderson (1985), respectively. Figure 1 shows a specific example for the temperature distribution of graphite grains embedded in a plasma with electron temperature $T_{\text{e}} = 10^8\ \text{K}$ and electron density $n_{\text{e}} = 10^{-3}\ \text{cm}^{-3}$. Note that the dust temperature is not uniquely specified for given electron temperature and density, but has a probability distribution depending on the grain size. For small ($a < 0.1\ \mu\text{m}$) grains, the cooling time gets shorter than the interval of collisions and the dust temperature has a large dispersion (so-called stochastic heating). Some portion of these grains can have rather high temperatures $\sim 100\ \text{K}$ owing to their small heat capacity. Larger grains, on the other hand, approach thermal equilibrium with ambient plasma and the temperature distribution has a sharp peak at $\sim 20\ \text{K}$. As a result of stochastic heating, the spectral shape of dust emission will be broadened particularly in the Wien regime. We will explicitly take into account such features in our prediction of the infrared emission from the ICD.

When dust grains are placed in a hot ICM, they are sputtered by impinging ions. We adopt the following analytic form for the sputtering rate (Tsai & Mathews 1995):

$$\frac{da}{dt} = -\tilde{h} \left(\frac{\rho_{\text{gas}}}{m_{\text{p}}} \right) \left[\left(\frac{T_{\text{s}}}{T_{\text{gas}}} \right)^{\omega} + 1 \right]^{-1}, \quad (1)$$

which gives a good approximation to the detailed calculations of Draine & Salpeter (1979) for both graphite and silicate grains when $\tilde{h} = 3.2 \times 10^{-18}\ \text{cm}^4\ \text{s}^{-1}$, $T_{\text{s}} = 2 \times 10^6\ \text{K}$, and $\omega = 2.5$. Using this formula, we define the sputtering timescale as

$$\tau_{\text{sputt}}(a, r) \equiv a |da/dt|^{-1}. \quad (2)$$

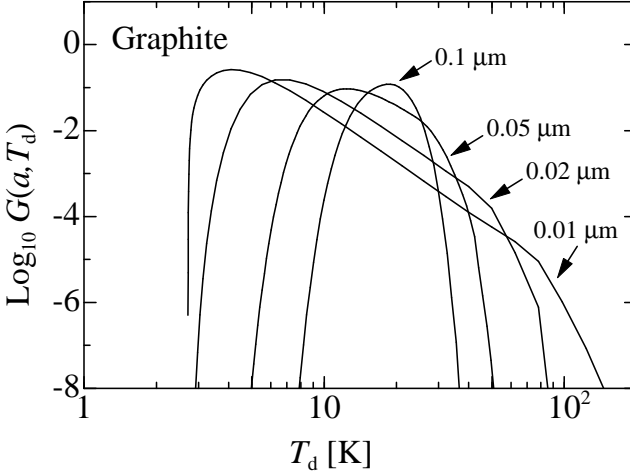


Fig. 1. Temperature distribution of graphite grains with various sizes embedded in a hot plasma with electron density 10^{-3} cm^{-3} and electron temperature 10^8 K .

For gas temperatures above $\sim 3 \times 10^6 \text{ K}$, the sputtering timescale is almost independent of gas temperature and approximated by

$$\tau_{\text{sputt}}(a, r) \sim 10^8 \left(\frac{a}{0.1 \mu\text{m}} \right) \left(\frac{n_e}{10^{-3} \text{ cm}^{-3}} \right)^{-1} \text{ yr.} \quad (3)$$

3.2. Size distribution of dust grains in the ICM

In modelling the size distribution of the ICD, we assume that the dust grains are continuously injected into the ICM from galaxies and destructed via sputtering. The size distribution $\partial n_i(a; r)/\partial a$ for species i at radial point r then follows (e.g., Dwek et al. 1990; Laor & Draine 1993)

$$\frac{\partial}{\partial a} \left(\dot{a} \frac{\partial n_i(a; r)}{\partial a} \right) + \frac{\partial}{\partial t} \frac{\partial n_i(a; r)}{\partial a} = \frac{\partial n_i^{\text{inj}}(a; r)}{\partial a} \tau_{\text{cluster}}^{-1}, \quad (4)$$

where $\dot{a} = da/dt$ is given by equation (1), $\partial n_i^{\text{inj}}(a; r)/\partial a$ describes the total number density of injected dust grains in the size interval between a and $a + \delta a$ at radial point r , and τ_{cluster} is the cluster lifetime over which dust grains have been injected. Neglecting uncertainties for the formation epochs of individual galaxies in clusters, we set τ_{cluster} equal to the age of the Universe at the cluster redshift. For the injected dust grains, we assume that they trace the galaxy distribution in a cluster and have the size distribution observed in our Galaxy (MRN):

$$\frac{\partial n_i^{\text{inj}}(a; r)}{\partial a} = A_i(r) a^{-\alpha^{\text{inj}}} \text{ for } a_{\text{min}} < a < a_{\text{max}}, \quad (5)$$

where $\alpha^{\text{inj}} = 3.5$, $a_{\text{min}} = 0.001 \mu\text{m}$, $a_{\text{max}} = 0.25 \mu\text{m}$, and $A_i(r) \propto \rho_{\text{gal}}(r)$ is the normalization coefficient to be determined later. Equation (4) is solved for steady-state to give

$$\frac{\partial n_i^{\text{std}}(a; r)}{\partial a} = A_i(r) \frac{a^{-\alpha^{\text{inj}}}}{\alpha^{\text{inj}} - 1} \frac{\tau_{\text{sputt}}(a, r)}{\tau_{\text{cluster}}}. \quad (6)$$

Since $\tau_{\text{sputt}} \propto a$, the steady-state size distribution is proportional to $a^{-\alpha^{\text{inj}} + 1}$.

Given large uncertainties in the galaxy distribution in each cluster, particularly at its outer envelope, we assume that galaxies trace collisionless dark matter and $A_i(r) \propto \rho_{\text{gal}}(r) \propto \rho_{\text{DM}}(r)$. We adopt the density profile of dark matter inferred from N-body simulations (Navarro, Frenk & White 1996, hereafter NFW):

$$\rho_{\text{DM}}(r) \propto \frac{1}{(r/r_s)(1 + r/r_s)^2} \quad (7)$$

where r_s is the scale radius of the halo. We follow Bullock et al. (2001) to determine r_s for a halo with virial mass M_{vir} at redshift z . As in Shimizu et al. (2003), we translate iteratively the scaled mass M_{500} , given for each cluster in Mohr et al. (1999) and Ota & Mitsuda (2004), into M_{vir} using the NFW profile, where M_{500} is the mass enclosed within the radius at which the mean density $\bar{\rho}(r)$ is equal to 500 times the critical density of the universe at the cluster redshift. The dark matter density is normalized by $M_{\text{vir}} = \int_0^{r_{\text{vir}}} \rho_{\text{DM}}(r) 4\pi r^2 dr$.

Taken together, $A_i(r)$ is determined by fixing the total amount of the injected dust grains $M_{\text{d}}^{\text{inj}}$ as

$$\begin{aligned} M_{\text{d}}^{\text{inj}}(< r_{\text{vir}}) &= \sum_i \frac{4\pi \rho_i}{3} \int_0^{r_{\text{vir}}} 4\pi r^2 A_i(r) dr \int_{a_{\text{min}}}^{a_{\text{max}}} a^{3-\alpha^{\text{inj}}} da \\ &= Z_{\text{d}}^{\text{inj}} Z_{\text{metal}} M_{\text{gas}}(< r_{\text{vir}}), \end{aligned} \quad (8)$$

where the injected dust-to-gas mass ratio $Z_{\text{d}}^{\text{inj}}$ is fiducially fixed at 0.0075 (MRN), and the mean metalicity Z_{metal} in units of the solar value is taken from Ota & Mitsuda (2004) and White et al. (2000). We have assumed that $Z_{\text{metal}} M_{\text{gas}}(< r_{\text{vir}})$ denotes the cumulative mass of the gas that has been supplied from galaxies into the ICM. Using the assumed relation of $A_i(r) \propto \rho_{\text{DM}}(r)$, we obtain

$$A_i(r) = \frac{3 f_i}{4\pi \rho_i} \frac{Z_{\text{d}}^{\text{inj}} Z_{\text{metal}}}{\int_{a_{\text{min}}}^{a_{\text{max}}} a^{3-\alpha^{\text{inj}}} da} \frac{M_{\text{gas}}(< r_{\text{vir}})}{M_{\text{vir}}} \rho_{\text{DM}}(r), \quad (9)$$

where f_i represents the mass fraction of graphite or silicate grains.

3.3. Infrared emission from the ICD

Given the size distribution (eq. [6]) and the temperature distribution $G_i(a, T_d)$ of the ICD, the infrared intensity at wavelength λ is given by an integral over the line-of-sight through the cluster:

$$\begin{aligned} I_{\lambda}(R) &= \sum_i \int_{-l_{\text{max}}}^{+l_{\text{max}}} dl \left[\int_{a_{\text{min}}}^{a_{\text{max}}} da \pi a^2 Q_{\lambda}^i(a) \frac{\partial n_i^{\text{std}}(a; r)}{\partial a} \right. \\ &\quad \times \left. \left\{ \int_{T_{\text{min}}}^{T_{\text{max}}} G_i(a, T_d) B_{\lambda}(T_d) dT_d \right\} \right], \end{aligned} \quad (10)$$

where $Q_{\lambda}^i(a)$ is the dust absorption efficiency factor of dust species i taken from Draine & Lee (1984), B_{λ} is the Planck function, R is the projected separation from the cluster center, and l is the length over a line of sight with $l_{\text{max}} = \sqrt{r_{\text{vir}}^2 - R^2}$. The minimum temperature of the dust T_{min} is set equal to the CMB temperature $2.73(1+z) \text{ K}$,

and the maximum temperature T_{\max} to the vaporization temperature, 2000 K for graphite and 1500 K for silicate, respectively (Dwek 1986). As $G_i(a, T_d)$ declines rapidly toward high temperatures, our results are insensitive to a specific choice of T_{\max} .

4. Results

4.1. Properties of the ICD

Based on the model constructed in the previous section, the ICD mass density as a function of physical radius r from the cluster center is given by

$$\rho_d(r) = \sum_i f_i \int_{a_{\min}}^{a_{\max}} \frac{4\pi a^3 \rho_i}{3} \frac{\partial n_i^{\text{std}}(a; r)}{\partial a} da. \quad (11)$$

The dust-to-gas mass ratio in the ICM can then be written as

$$Z_d(r) = \frac{\rho_d(r)}{\rho_{\text{gas}}(r)}. \quad (12)$$

We define the mass weighted mean temperature and mean size of the ICD as follows:

$$\langle T_d(r) \rangle = \left[\sum_i f_i \int_{a_{\min}}^{a_{\max}} \left\{ \int_{T_{\min}}^{T_{\max}} G_i(a, T_d) T_d dT_d \right\} \times \frac{4\pi a^3 \rho_i}{3} \frac{\partial n_i^{\text{std}}(a; r)}{\partial a} da \right] / \rho_d(r), \quad (13)$$

$$\langle a_d(r) \rangle = \left[\sum_i f_i \int_{a_{\min}}^{a_{\max}} \frac{4\pi a^3 \rho_i}{3} \times \frac{\partial n_i^{\text{std}}(a; r)}{\partial a} da \right] / \rho_d(r). \quad (14)$$

For later convenience, we further introduce the surface mass density of the ICD at a projected separation R from the cluster center by

$$\Sigma_d(R) = \int_{-l_{\max}}^{+l_{\max}} \rho_d(r) dl. \quad (15)$$

Figures 2–4 show the above quantities in a specific case of Perseus cluster (A426). As will be shown below, the expected intensity from this cluster is among the highest in our entire sample and we will take it as a representative target in our subsequent analysis. The dust-to-gas mass ratio $Z_d(r)$ is lower, particularly near the center, by several orders of magnitude than the Galactic value 0.0075 as a result of rapid sputtering (Fig. 2). The mean dust temperature $\langle T_d(r) \rangle$, on the other hand, is the highest near the center at > 30 K due to efficient heating by electron collisions (Fig. 3). The mean size of the dust is independent of r and its value in Perseus is $\sim 0.15 \mu\text{m}$. Once integrated over the line-of-sight, the ICD surface mass density Σ_d remains nearly constant within the projected separation of ~ 300 kpc (Fig. 4) and will serve as a good measure of the total amount of the ICD.

4.2. Expected infrared spectra

We plot the predicted ICD emission spectra from Perseus cluster in Figure 5. In the rest of the paper,

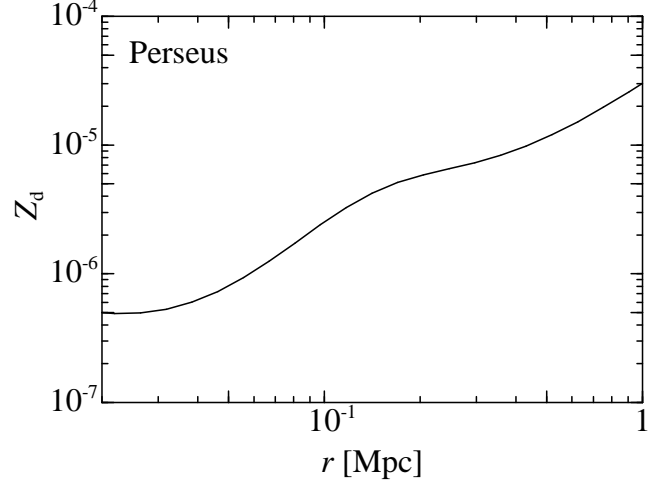


Fig. 2. Dust-to-gas mass ratio in the ICM of Perseus cluster (A426) as a function of physical radius from the center.

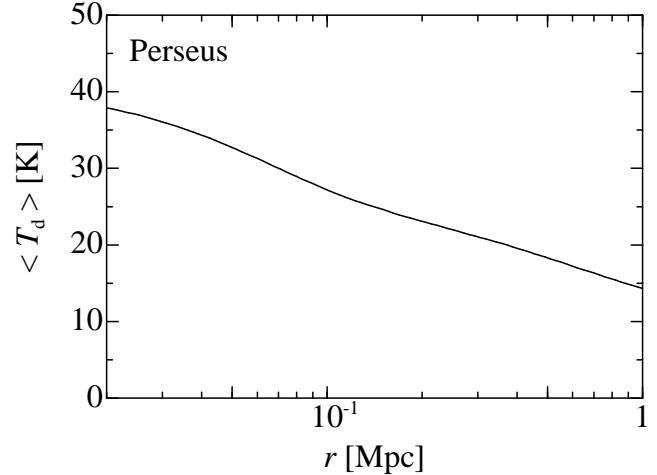


Fig. 3. Mass weighted mean temperature of the ICD in Perseus as a function of physical radius from the center.

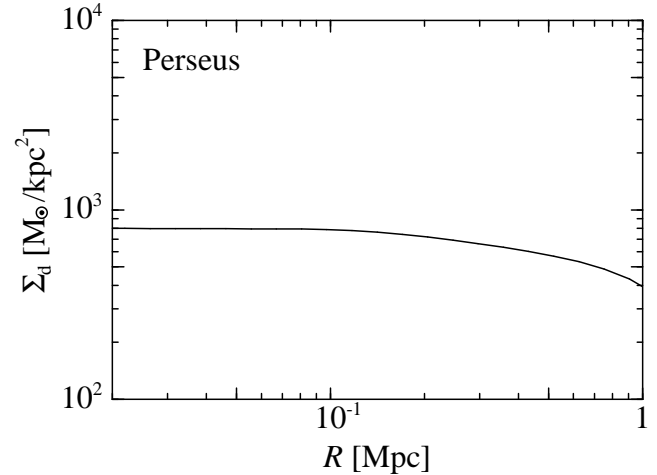


Fig. 4. Surface mass density of the ICD in Perseus as a function of projected separation from the cluster center.

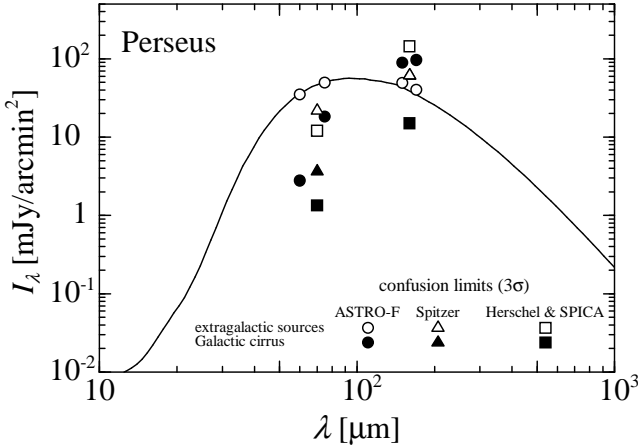


Fig. 5. Predicted spectra of the ICD at the projected separation of 20 kpc from the center of Perseus cluster. Open circles, open triangles and open squares show the 3σ confusion limits, due to extragalactic sources, for ASTRO-F, Spitzer, Herschel and SPICA missions, respectively. Filled symbols with an identical shape indicate those due to Galactic cirrus for the same instrument. Note that the open and filled triangles overlap each other at 160 μm .

unless otherwise stated explicitly, the emission is computed at the projected separation of 20 kpc from the center in order to avoid any contamination from the central galaxy. Also plotted for reference are the 3σ confusion limits due to extragalactic sources, for Spitzer/MIPS (Dole et al. 2004), ASTRO-F/FIS (Pearson et al. 2004), Herschel and SPICA (Dole et al. 2004), as well as those due to Galactic cirrus (Jeong et al. 2005). The confusion levels are computed at the beam size of each instrument. For simplicity, we represent band filters of FIS (N60, N170, WIDE-S and WIDE-L) by their central wavelengths 60, 170, 75 and 150 μm , respectively. We adopt 70 μm and 160 μm for the band filters of Herschel and SPICA. The PSF of each instrument is modeled by a Gaussian with the FWHM value taken from the reference mentioned above. We also take into account the dependence of the cirrus emission on the Galactic latitude as in Jeong et al. (2005). The total confusion limit should be estimated as $\sigma_{\text{tot}} = \sqrt{\sigma_{\text{extragalactic}}^2 + \sigma_{\text{cirrus}}^2}$. This figure indicates that the source confusion is dominated by extragalactic sources at $\lambda < 100 \mu\text{m}$, while the contribution of Galactic cirrus increases rapidly at longer wavelengths. The predicted emission has its peak at $\sim 70 - 100 \mu\text{m}$ and would be detectable above 5σ levels at 70 μm with Spitzer, Herschel and SPICA, and marginally detectable at the 3σ levels at 60 and 75 μm with ASTRO-F.

Figure 6 shows the expected radial profiles for the emission from Perseus. The emission at 70 μm would be detectable above the 3σ levels within ~ 2.5 arcmin by Spitzer and within ~ 4.5 arcmin by Herschel and SPICA. At the outer envelopes of the cluster, the emission declines owing to the lack of hot gas capable of heating the dust. The extended feature of the emission will be of particular importance in separating the ICD component from galaxies.

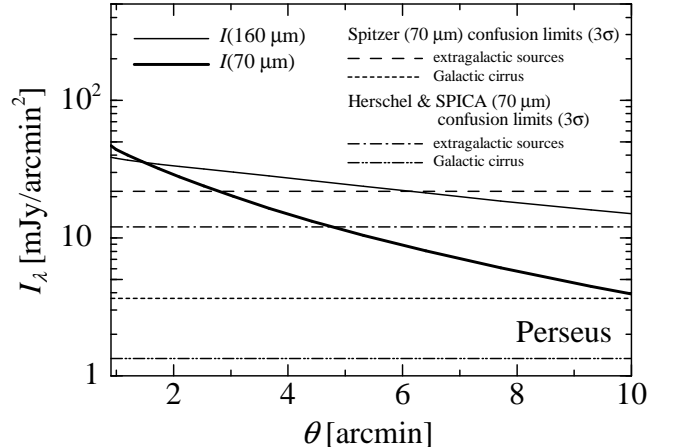


Fig. 6. Expected radial profiles of the ICD emission at 70 μm (thick solid line) and 160 μm (thin solid line) in Perseus cluster. Also plotted for reference are the 3σ confusion limits at 70 μm ; extragalactic sources for Spitzer (dashed line), Herschel and SPICA (dash-dotted line), and Galactic cirrus for Spitzer (dotted line), Herschel and SPICA (dash-dot-dotted line).

A fine spatial resolution of Spitzer, ASTRO-F, Herschel and SPICA will be essential for this purpose.

In Figure 7, we plot the expected intensities of the ICD for the entire sample of clusters as a function of the Galactic latitude. In general, the highest signal-to-noise ratio (S/N) is achieved at 70 μm . Five clusters with the highest 70 μm intensity (filled symbols) all lie above the 4σ levels for Spitzer and above the 7σ levels for Herschel and SPICA. The emission tends to decrease toward high redshift because the observed intensity and wavelength vary as $\propto (1+z)^{-4}$ and $\propto 1+z$, respectively. Several nearby clusters at $z < 0.1$ lie above the 3σ levels of the detector at 70 μm , 150 μm , and 170 μm . They are likely to serve as plausible candidates for the positive detection of the ICD.

We note that the confusion noise per beam, due to extragalactic sources, drops slower than the size of the aperture squared at $\lambda > 100 \mu\text{m}$ (e.g., Dole et al. 2004). This makes the extragalactic confusion per fixed sky area *increase* with an increasing telescope size (Figs 5 and 7). At such long wavelengths, one may be able to achieve higher S/N by adding together the larger sky area, while high resolution detectors should still be useful to exclude individual galaxies.

In order to examine the scale dependence of the ICD detectability, we plot in Figure 8 the average surface brightness of A3571 at 160 μm within a given radius excluding the central 20 kpc region. Also plotted for reference are the confusion levels for the same area. We have chosen A3571 because it has the highest S/N at 160 μm among the five representative clusters mentioned above. In computing the confusion noises for larger sky area, we have extrapolated the values indicated in Table 1 and 2 of Dole et al. (2004) for extragalactic sources and Figure 17 of Jeong et al. (2005) for Galactic cirrus, respectively. The extragalactic noise drops more rapidly with scale than the cluster signal, while the Galactic confusion increases

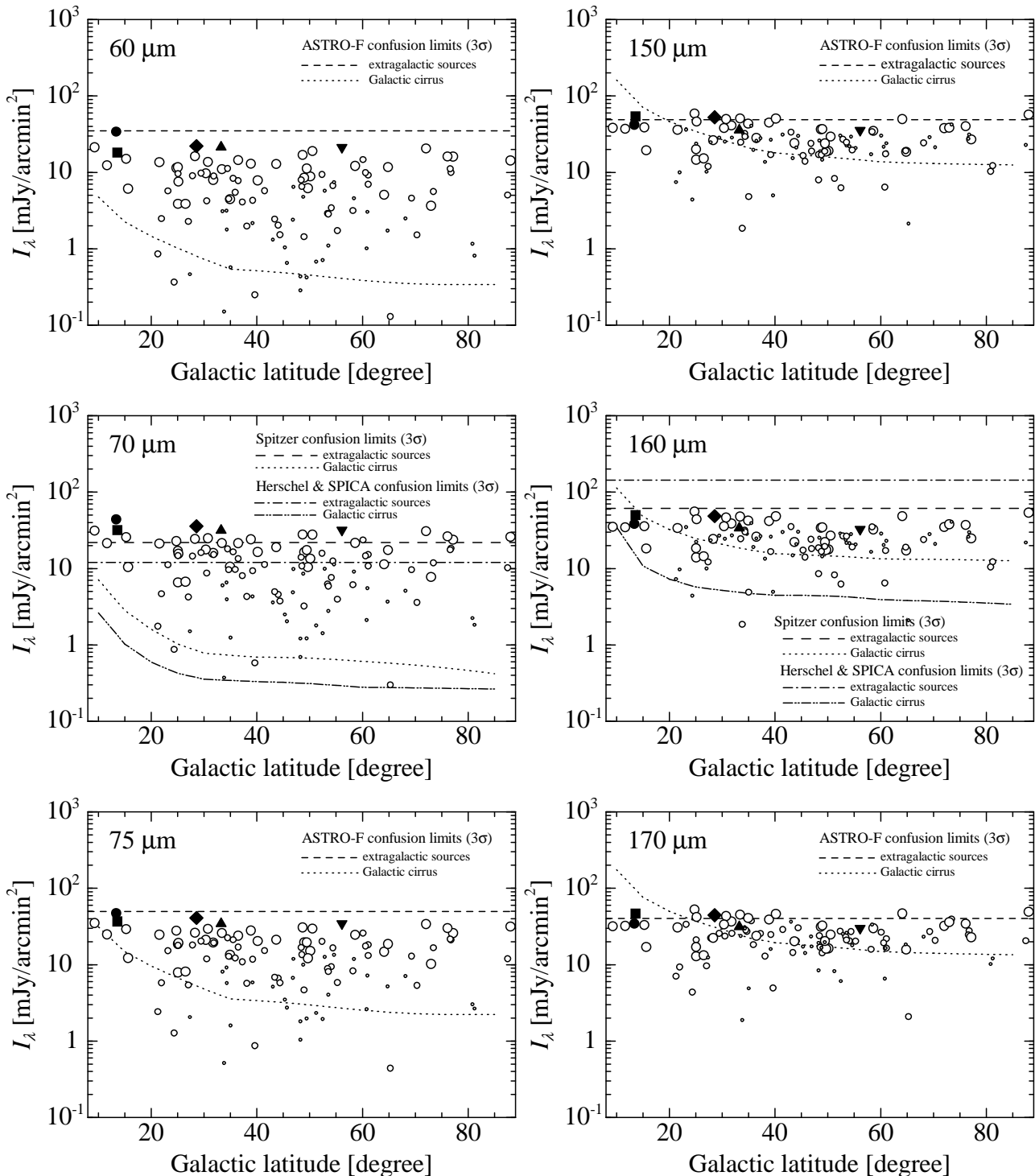


Fig. 7. Expected intensities at 60, 70, 75, 150, 160 and 170 μm at the projected separation of 20 kpc from the center of 117 galaxy clusters versus Galactic latitude. Five clusters with the highest 70 μm intensities are marked by filled symbols; Perseus (circle), A2319 (square), A3571 (lozenge), A2204 (triangle), and A3112 (reverse-triangle). The other clusters are marked by open circles; at redshift $0.01 < z < 0.1$ (large circles), at $0.1 \leq z < 0.3$ (medium circles), and at $0.3 \leq z < 0.8$ (small circles). Lines represent 3 σ confusion limits, due to extragalactic sources and Galactic cirrus for the mission indicated in each panel.

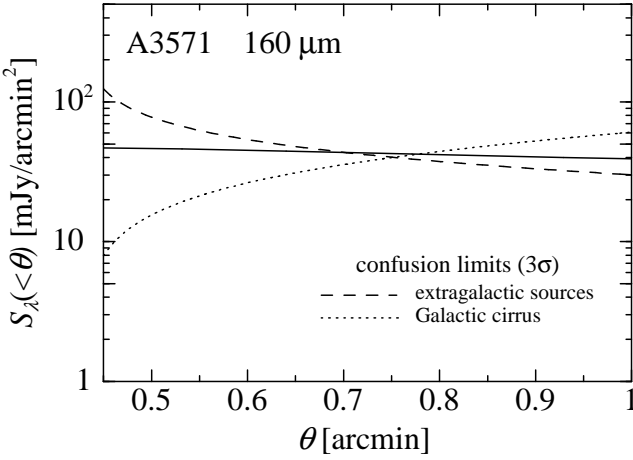


Fig. 8. Average surface brightness of A3571 at 160 μm within a given radius excluding the central 20 kpc region. Also plotted for reference are the confusion levels at 160 μm for the same area; due to extragalactic sources (dashed line) and Galactic cirrus (dotted line).

monotonically. The highest S/N is expected within $\theta \sim 45$ arcsec. This sort of multi-scale analysis is a powerful tool for detecting the ICD at $> 100 \mu\text{m}$.

4.3. Constraints on the ICD properties

We have so far assumed that the dust has been injected into the ICM with essentially the same size distribution and amount as in our Galaxy. We now examine how sensitive our results are to their uncertainties and explore what constraints one can place in turn on the underlying dust model from future observations.

Specifically, we vary three parameters in our model; the power-law index α of the dust size distribution, their maximum size a_{\max} , and the surface mass density Σ_d at the projected radius $R = 20$ kpc. Since very small dust grains are rapidly destroyed in the ICM and do not contribute to mid- to far-infrared emissions, we simply fix the minimum dust size at $a_{\min} = 0.001 \mu\text{m}$. As mentioned in Section 3, the power-law index α is related to that of the injected dust with $\alpha = \alpha^{\text{inj}} - 1$ and has the value 2.5 for $\alpha^{\text{inj}} = 3.5$ (MRN). As shown in Figure 4, Σ_d is nearly constant in the cluster and serves as a good measure for the total amount of the ICD. We take Perseus as a representative target and use the data at 24, 70 and 160 μm to derive constraints on the three parameters mentioned above.

Figure 9 shows contours of the 70 μm intensity on $a_{\max} - \Sigma_d$ plane for $\alpha = 2.5$ and $\alpha - \Sigma_d$ plane for $a_{\max} = 0.25 \mu\text{m}$. We find that the intensity is much more sensitive to Σ_d than to a_{\max} and α . This indicates that the detection of (or an upper limit to) the ICD emission directly leads to a measure of the total amount of dust almost independently of its size distribution. Note that the mean ICD temperature varies only moderately and can be well constrained once electron density and temperature are known from X-ray observations (Fig. 3).

Constraints on the size distribution, a_{\max} and α , will be obtained via multi-band observations as illustrated in

Figure 10. Since the intensities are proportional to Σ_d , uncertainties in Σ_d are eliminated by taking their ratios in multi-bands. The ratio $I(160 \mu\text{m})/I(70 \mu\text{m})$ can yield a reasonable measure of a_{\max} provided that α is not significantly different from that inferred in the MRN model $\alpha = 2.5$. On the other hand, $I(24 \mu\text{m})/I(70 \mu\text{m})$ is more sensitive to α than a_{\max} and can be used to infer the former quantity if sufficient S/N is achieved in both bands.

5. Discussion

There have been a number of suggestions as to how dust grains are replenished into the intergalactic medium. For example, many authors have argued that a significant amount of dust could be expelled from galaxies by radiation pressure (e.g., Chiao & Wickramasinghe 1972; Ferrara et al. 1991; Shustov & Vibe 1995; Davies et al. 1998; Simonsen & Hannestad 1999; Aguirre et al. 2001a,b). Radiation pressure may limit the injected dust size at 0.05 – 0.2 μm (Shustov & Vibe 1995 ; Davies et al. 1998) because smaller grains are rapidly destroyed via sputtering in galactic halos while larger ones are hard to escape from the gravitational potential of galaxies. Ejection of small grains can be suppressed further by drag forces due to dust-gas collisions and Coulomb interactions (Bianchi & Ferrara 2005). Ferrara et al. (1991) point out that radiation pressure may also change the composition of ejected grains because graphite grains can attain higher velocities and escape more easily from galaxies than silicate grains.

Another potential source of the ICD is from the intracluster stellar population (Montier & Giard 2004). Zwicky (1951) was the first to suggest the presence of the intracluster stars based on the detection of the excess light between the galaxies of the Coma cluster. Numerical simulations indicate that ~ 10 – 20 per cent of the total cluster light should be the ICM (Murante et al. 2004; Willman et al. 2004). Recently, planetary nebula (e.g. Feldmeier et al. 2004; Theuns & Warren 1997), red-giant-branch stars (Ferguson et al. 1998; Durrell et al. 2002), and also Type Ia supernova (Gal-Yam et al. 2003) have been detected in the ICM. The amount of intracluster light allowed from these observations is ~ 10 – 50 per cent of the total cluster light. According to Montier & Giard (2004), the dust-to-gas mass ratio of the Coma-like cluster, due to the intracluster stellar population, is $\sim 10^{-5}$ within a radius of 1 Mpc and predominant compared to the galactic production. The intracluster stellar population can add small dust and silicate grains that might be suppressed if galaxies are the only source of the ICD. As demonstrated in Section 4.3, multi-band observations of the dust emission will provide a powerful probe of the grain size distribution, which can be used to constrain the ejection processes of the ICD.

6. Conclusions

In this paper, we have performed a comprehensive study on the nature of diffuse dust in a sample of galaxy clusters

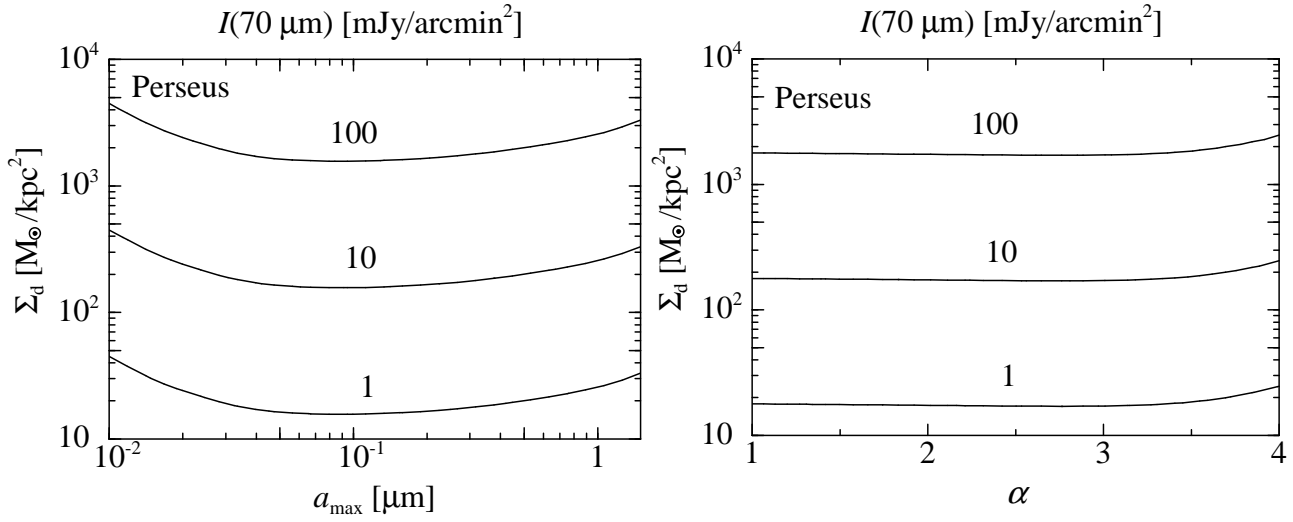


Fig. 9. Contours of the $70 \mu\text{m}$ intensity from Perseus on an $a_{\text{max}} - \Sigma_d$ plane for $\alpha = 2.5$ (left panel) and an $\alpha - \Sigma_d$ plane for $a_{\text{max}} = 0.25 \mu\text{m}$ (right panel). The curves correspond to $I(70 \mu\text{m}) = 100, 10$ and 1 mJy/arcmin^2 from top to bottom in the both panels.

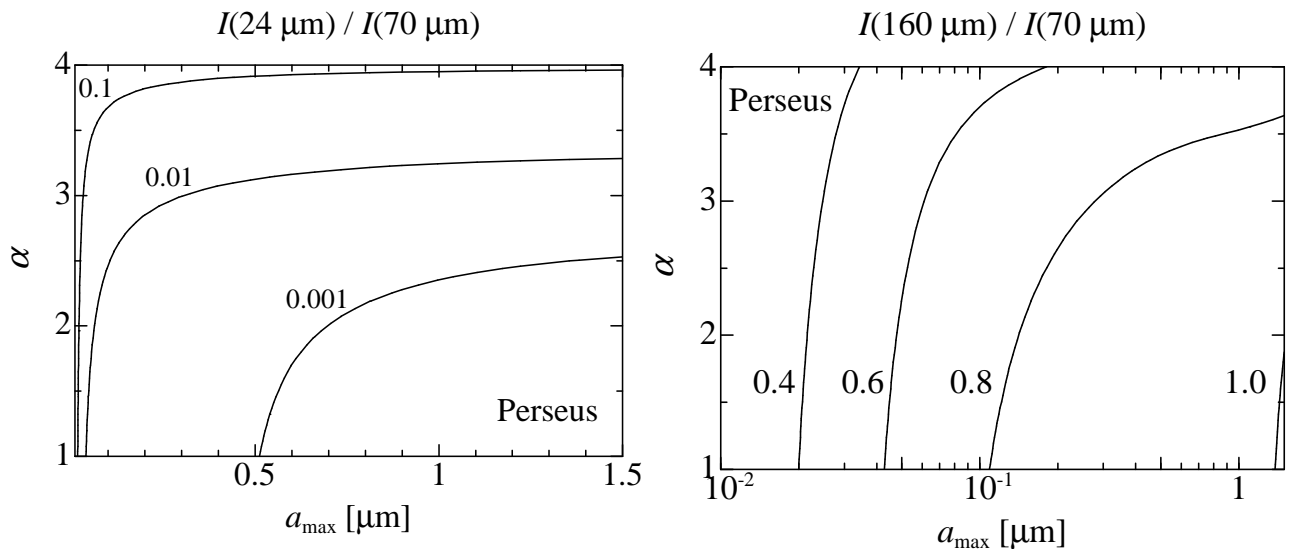


Fig. 10. Contours of the intensity ratios, $I(24 \mu\text{m})/I(70 \mu\text{m})$ (left panel) and $I(160 \mu\text{m})/I(70 \mu\text{m})$ (right panel) on an $a_{\text{max}} - \alpha$ plane for Perseus. The curves, from top to bottom, correspond to $I(24 \mu\text{m})/I(70 \mu\text{m}) = 0.1, 0.01$ and 0.001 in the left panel and to $I(160 \mu\text{m})/I(70 \mu\text{m}) = 0.4, 0.6, 0.8$ and 1.0 in the right panel.

at redshift $z \sim 0.01 - 0.8$. Based upon recent X-ray data, the temperature distribution of the dust grains are computed taking account of collisional heating by ambient hot plasma and radiative cooling. The dust size distribution is also solved by incorporating injection from galaxies and destruction via sputtering.

If the dust grains are injected into the intergalactic medium with the amount and size comparable to the Galactic values, the dust-to-gas ratio is typically $\sim 10^{-6}$ and the mean dust temperature is ~ 30 K near the cluster center. The predicted emissions lie marginally above the detection thresholds for Spitzer Space Telescope, ASTRO-F, Herschel and SPICA missions. The highest signal-to-noise ratios ($> 4\sigma$) are expected for some nearby clusters such as Perseus, A3571, A2319, A3112 and A2204 at the $70 \mu\text{m}$ band.

Given rather tight constraints on the dust temperature from observed electron density and temperature, the dust mass can be inferred directly from the infrared observations. Further constraints on the size distribution will be obtained once multi-band data are available by the future facilities. They will definitely provide a powerful probe of the dust injection processes and dust-gas interactions in the intergalactic space.

We thank Woong-Seob Jeong for offering the confusion noise data due to Galactic cirrus, Naomi Ota for providing the X-ray data of distant clusters, and the referee Martin Giard for helpful comments. We also thank Hidehiro Kaneda, Hirohisa Nagata, Mamoru Shimizu, and Hidenori Takahashi for useful discussions. This work is supported in part by the Grants-in-Aid by the Ministry of Education, Science and Culture of Japan (14740133:TK).

References

Aguirre, A., Hernquist, L., Katz, N., Gardner, J., & Weinberg, D. 2001a, *ApJ*, 556, L11

Aguirre, A., Hernquist, L., Schaye, J., Katz, N., Weinberg, D. H., & Gardner, J. 2001b, *ApJ*, 556, 521

Arnaud, K. A., & Mushotzky, R. F. 1998, *ApJ*, 501, 119

Bianchi, S., & Ferrara, A. 2005, *MNRAS*, 358, 379

Bullock, J. S., Kolatt, T. S., Sigad, Y., Somerville, R. S., Kravtsov, A. V., Klypin, A. A., Primack, J. R., & Dekel, A. 2001, *MNRAS* 321, 559

Buote, D. A. 2000, *MNRAS*, 311, 176

Chiao, R. Y., & Wickramasinghe, N. C. 1972, *MNRAS*, 159, 361

Davies, J. I., Alton, P., Bianchi, S., & Trehewella, M. 1998, *MNRAS*, 300, 1006

Davis, D. S., Mulchaey, J. S., & Mushotzky, R. F. 1999, *ApJ*, 511, 34

Dole, H., Lagache, G., & Puget, J. L. 2003, *ApJ*, 585, 617

Dole, H., et al. 2004, *ApJS*, 154, 93

Draine, B. T., & Anderson, N. 1985, *ApJ*, 292, 494

Draine, B. T., & Lee, H. M. 1984, *ApJ*, 285, 89

Draine, B. T., & Salpeter, E. E. 1979, *ApJ*, 231, 77

Durrell, P. R., Ciardullo, R., Feldmeier, J. J., Jacoby, G. H., & Sigurdsson S. 2002, *ApJ*, 570, 119

Dwek, E. 1986, *ApJ*, 302, 363

Dwek, E., Rephaeli, Y., & Mather, J. C. 1990, *ApJ*, 350, 104

Feldmeier, J. J., Ciardullo, R., Jacoby, G. H., & Durrell, P. R. 2004 *ApJ*, 615, 196

Ferguson, H. C., Tanvir, N. R., & von Hippel, T. 1998, *Nature*, 391, 461

Ferrara, A., Ferrini, F., Franco, J., & Barsella, B. 1991, *ApJ*, 381, 137

Gal-Yam, A., Maoz, D., Guhathakurta, P., & Filippenko, A. V. 2003, *AJ*, 125, 1087

Girardi, M., Mezzetti, M., Giuricin, G., & Mardirossian, F. 1992, *ApJ*, 394, 442

Goudfrooij, P., & de Jong, T. 1995, *ApJ*, 298, 784

Hickson, P., Menon, T. K., Palumbo, G. G. C., & Persic, M. 1989, *ApJ*, 341, 679

Jeong, W.-S., Lee, H. M., Pak, S., Nakagawa, T., Kwon, S. M., Pearson, C. P., & White, G. J. 2005, *MNRAS*, 357, 535

Karachentsev, I. D., & Lipovetskii, V. A. 1969, *Soviet Phys.*, 12, 909

Kitayama, T., Komatsu, E., Ota, N., Kuwabara, T., Suto, Y., Yoshikawa, K., Hattori, M., & Matsuo, H. 2004, *PASJ*, 56, 17

Komatsu, E., Kitayama, T., Suto, Y., Hattori, M., Kawabe, R., Matsuo, H., Schindler, S., & Yoshikawa K. 1999, *ApJ*, 516, L1

Laor, A., & Draine, B. T. 1993, *ApJ*, 402, 441

Li, A., & Draine, B. T. 2001, *ApJ*, 554, 778

Maoz, D. 1995, *ApJ*, 455, L115

Mathis, J. S., Rumpl, W., & Nordsieck, K. H. 1977, *ApJ*, 217, 425

Mohr, J. J., Mathiesen, B., & Evrard, A. E. 1999, *ApJ*, 517, 627

Montier, L. A., & Giard, M. 2004, *A&A* 417, 401

Montier, L. A., & Giard, M. 2005, accepted for publication in *A&A*

Murante G., et al. 2004, *ApJ*, 607, L83

Mushotzky, R., Loewenstein, M., Arnaud, K. A., Tamura, T., Fukazawa, Y., Mastushita, K., Kikuchi, K., & Hatsukade, I. 1996, *ApJ*, 466, 686

Navarro, J. F., Frenk, C. S., & White, S. D. M. 1996, *ApJ*, 462, 563

Ota, N., & Mitsuda, K. 2004, *A&A* 428, 757

Pearson, C. P., et al. 2004, *MNRAS*, 347, 1113

Renzini, A. 1997, *ApJ*, 488, 35

Shimizu, M., Kitayama, T., Sasaki, S., & Suto Y. 2003, *ApJ*, 590, 197

Shustov, B. M., & Vibe, D. Z. 1995, *Astronomy Reports*, 39, 578

Simonsen, J. T., & Hannestad, S. 1999, *A&A*, 351, 1

Stickel, M., Lemke, D., Mattila, K., Haikala, L. K., & Haas, M. 1998, *A&A*, 329, 55

Stickel, M., Klaas, U., Lemke, D., & Mattila, K. 2002, *A&A*, 383, 367

Sulentic, J. W., & De Mello Rabaca, D. F. 1993, *ApJ*, 410, 520

Theuns, T., & Warren, S. J. 1997, *MNRAS*, 284, L11

Tsai, J. C., & Mathews, W. G. 1995, *ApJ*, 448, 84

White, D. A. 2000, *MNRAS*, 312, 663

Willmanet, B., Governato, F., Wadsley, J., & Quinn T. 2004, *MNRAS*, 355, 159

Yoshikawa, K., & Suto, Y. 1999, *ApJ*, 513, 549

Zwicky, F. 1951, *PASP*, 63, 61

Zwicky, F. 1962, in *Problems in Extragalactic Research*, ed. G. C. McVittie(New York:Macmillan), 149